Journal of Aerospace Information Systems
Vol. 19, No. 5, May 2022

Load-Distribution-Based Trajectory Planning and Control for a Multilift System

Junyi Geng*
Carnegie Mellon University, Pittsburgh, Pennsylvania 15213
and
Puneet Singla† and Jack W. Langelaan†
Pennsylvania State University, University Park, Pennsylvania 16802

https://doi.org/10.2514/1.I011067

This paper studies a load-distribution-based trajectory planning and control strategy for a hierarchically controlled multilift system. It proposes a method that simultaneously plans payload trajectory and cable forces while satisfying path and force constraints and minimizing the difference in cable forces. A direct collocation method is used to solve the formulated planning problem. Then, a neighboring feedback law is designed to equalize the cable tension load distribution during flight. Here, the system dynamics are linearized about the nominal path. An linear-quadratic regulator (LQR) controller is then designed for the system to track the planned trajectory. Simulations of payload transport showed that even with the effect of disturbances (i.e., wind gusts), cable tensions are more evenly distributed with the proposed approach. Finally, indoor flight tests were performed to validate the proposed approach. Results showed that the system has reduced energy consumption compared with the case without planning based on load distribution. The rotorcraft achieved less average total power and near-equal energy consumption.

I. Introduction

THE general case of multilift consists of multiple rotorcraft cooperatively carrying a single slung payload. This concept of multilift increases the utility of a fleet of small rotorcraft by enabling the transport of large, heavy payloads via coordinated transport. Besides their payload capacity, which frees us from building larger and higher-lifting-capacity rotorcraft that would rarely be used but costly, such systems have several advantages: mission redundancy, robustness, and provision for overall task efficiency improvement.

Based on the control strategy, the state-of-the-art can be classified into two groups: rotorcraft based (or decentralized multilift) and payload based (or centralized multilift). In the decentralized case, the rotorcraft fly along some trajectories while carrying an external payload. The slung load is treated as an external force or disturbance that has a known value or known bound. Path generation is performed usually for the rotorcraft based on the multilift formation and the quasi-static payload [1–3], which neglects the payload dynamics. In the centralized case, efforts are mainly focused on the payload dynamics and control. Rotorcraft perform as the actuators driving the payload to the desired states [4–7]. The trajectory of rotorcraft can be computed either based on the flat output by specifying the payload trajectory of the load up to the sixth derivative in position and up to the fourth derivative in orientation [4] or based on the payload feedback by computing the cable force in real time and then command the rotorcraft using the direct kinematic relation between payload and rotorcraft [5,8].

In the case of a homogeneous fleet of rotorcraft carrying a payload, it is intuitively appealing to operate the vehicles at near-equal load (e.g., near-equal cable tension) so that all vehicles have similar control overhead and so that all vehicles operate at near-equal energy consumption, leaving little room for unequal load distribution to maximize the power benefit [9,10]. If one of the rotorcraft takes the major part the load, this would lead to an inefficient global performance for the whole system. Although significant work has been done in modeling the multilift dynamics [11], developing control strategies [1,12–15] to make multilift flight feasible and robust to the uncertainty [16], and creating estimation methods for slung load states or parameters [17–20], comparatively little work has been done in control strategies or planning methods that ensure equal load distribution. Enciu and Horn [9] performed a numeric optimization for maximizing the cruise performance of a multilift system with four rotorcraft focusing on the control side instead of trajectory planning. Relative distance between the formation rotorcraft, airspeed, and cable length were shown to have influence on the optimization results. In [10,21], Berrios et al. investigated the load distribution control concept for a dual-lift system to equalize the cable tension between the two cables. A swing angle feedback controller was designed, which increased the damping ratio of the external payload's swinging motion. Results showed that a system with load distribution control can reduce the tracking error significantly.

Recently, a hardware implementation [22,23] using four quadrotor robots carrying a single slung load was performed based on a hierarchical approach [8]. Flight tests conducted in an indoor motion-capture studio demonstrated performance of the system. A preplanned payload trajectory was parameterized using polynomial curve method.

Despite previous efforts [10,21,24], load-distribution-based trajectory planning for multilift (i.e., more than two cooperative vehicles) is less well-explored. Therefore this paper has two main foci. First is formulation of an optimal control problem that preplans both the multilift slung load trajectory and cable forces while satisfying path and force constraints while minimizing variance in cable tension. Second is design of a feedback control law to track this trajectory during flight. Simulation results that include external disturbance (i.e., gusts) are presented to verify the proposed method. Finally, hardware flight tests are performed indoor to validate the proposed planning and control strategy, showing the comparison of the system with or without planning based load distribution.

The rest of this paper is organized as follows: In Sec. II, the cooperative transportation problem and the multilift system are introduced. The load-distribution-based planning and tracking problem are also formulated. The analysis and methodology including the direct collocation method and the neighboring feedback control are described in Sec. III. Simulation results that include wind gust are presented in Sec. IV. Then, Sec. V provides the hardware flight tests

Presented as Paper 2021-0980 at the AIAA SciTech 2021 Forum, Guidance, Navigation, and Control, Virtual Event, January 11–21, 2021; received 25 September 2021; revision received 21 December 2021; accepted for publication 4 January 2022; published online 8 February 2022.

*Postdoctoral Fellow, Robotics Institute; junyigen@andrew.cmu.edu.
†Professor, Department of Aerospace Engineering. Associate Fellow AIAA.

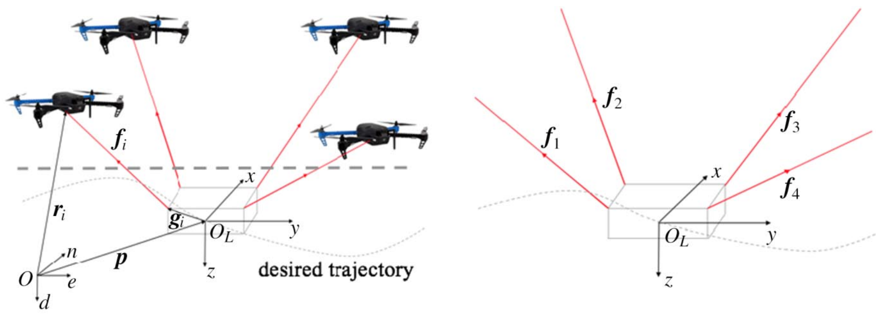

a) Schematic of the multilift b) Free body diagram

Fig. 1 Multilift problem and simplification.

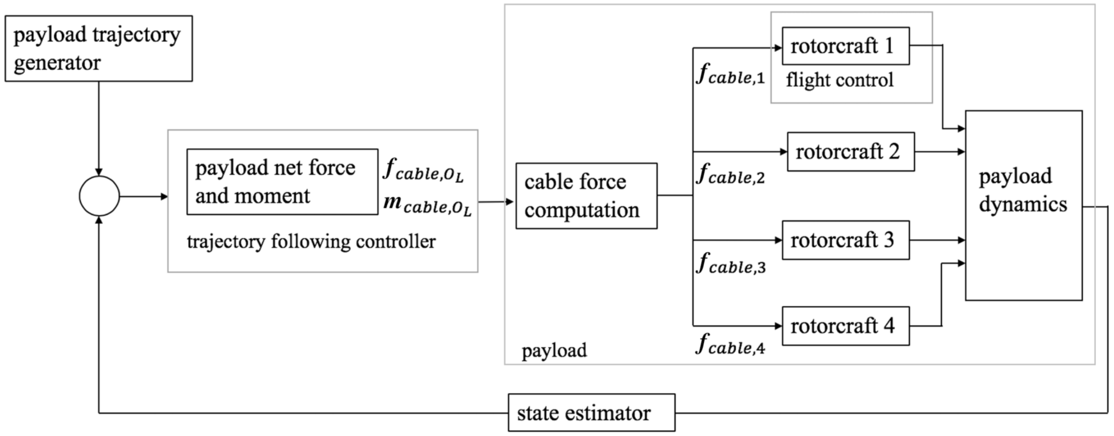

Fig. 2 Multilift system block diagram.

in an indoor motion capture studio validating the proposed approach. Finally, concluding remarks are given in Sec. VI.

II. Problem Formulation

The problem considered here is transporting a slung load by a team of four autonomous rotorcraft; see Fig. 1a. The task of the rotorcraft is to ensure that the payload can follow the desired trajectory.

Referring to Fig. 1a, the payload is located at $\boldsymbol{p}$ in a world fixed frame $\mathcal{F}_e = \{\mathcal{O}_e, \boldsymbol{\mathcal{X}}_e, \boldsymbol{\mathcal{Y}}_e, \boldsymbol{\mathcal{Z}}_e\}$. The pose of the payload is described by the vector $\boldsymbol{x}_L = [\boldsymbol{p}^T, \boldsymbol{\Omega}^T]^T \in SE(3)$ that represents position $\boldsymbol{p} \in \mathbb{R}^3$ and orientation $\boldsymbol{\Omega} \in SO(3)$ of a frame $\mathcal{F}_L = \{\mathcal{O}_L, \boldsymbol{\mathcal{X}}_L, \boldsymbol{\mathcal{Y}}_L, \boldsymbol{\mathcal{Z}}_L\}$. The rotation matrix from $\mathcal{F}_e$ to $\mathcal{F}_L$ $\boldsymbol{R}_{e2L}$ is a function of 3-2-1 Euler angles $\boldsymbol{\Omega} = [\phi, \theta, \psi]^T$. A team of four rotorcraft located at $\boldsymbol{r}_i$, $i = 1, \ldots, 4$, in the frame $\mathcal{F}_e$ are connected to the payload with individual cables attached to the payload at connection points $\boldsymbol{g}_i$ in frame $\mathcal{F}_L$.

The hierarchical approach is described in detail in [8,22,23] and is shown in Fig. 2. A trajectory generator generates the desired trajectory of the payload. This can be precomputed or come from a human operator. Upon receiving the desired payload states, the trajectory following controller computes the desired net force and moment acting on the payload to "steer" the payload from its current state to the desired states. Individual cable force for each tether is computed based on the net force and moment and the geometry of the cable attachments on the payload. In the implementation presented there, the cable force computation uses least-norm solution to satisfy the net forces and moments and uses the null space to satisfy constraints on the system such as vehicle separation and controllability. The desired rotorcraft states can then be computed based on these cable force vectors and physical properties of the cables. A flight controller onboard each rotorcraft ensures that the required cable force can be maintained. Figure 3 shows the system in operation in an indoor motion capture studio.

The key part of this approach is computing the set of required cable forces. Given the cable forces (i.e., tension and direction), the desired rotorcraft states (i.e., position, velocity, and acceleration) can be determined through the direct kinematics relation between payload and rotorcraft. Assuming that the rotorcraft can respond instantly to commands for some bounded set of cable forces, one can treat the system as a rigid-body motion with a set of cable forces as inputs (Fig. 1b).

The focus of this paper is on the payload trajectory generation. The goal is to find a trajectory, including the payload states and input sequence, and the corresponding control mechanism to achieve evenly distributed load on each tether when flying from given waypoints A to B in a fixed amount of time while satisfying the payload equation of motion and the input constraints. This essentially combines the trajectory generator, the trajectory following controller, and the cable force computation blocks of Fig. 2. To achieve this goal, the problem is split into two parts: 1) preplan a desired trajectory for the payload and cable force while considering the load distribution for the ideal environment; 2) design a feedback controller for the system to track the desired reference trajectory under disturbance.

Assumption 1: In this study, payload trajectories with small pitch and roll angles are considered since the near-hover case was successfully tested in hardware flight [22,23]; see Fig. 3. Large slung load maneuver (greater than 10 deg pitch and roll) is beyond the scope of this paper.

Assumption 2: The cables are always in tension.[‡] Cable force vectors remain in the same quadrant within a fixed sector region $\Delta\beta$ [22,23] (see Fig. 4) in the payload body frame so that cables will not cross and ensure vehicle separation. Note that $\Delta\beta$ does not affect the payload controllability as long as the four cables remain within different quadrants [25]. The cone angle α_i between each cable and

[‡]For the cooperative aerial slung load application, the rotorcraft and the payload stay in the air for most of the time with small maneuver. Because big maneuver will be hazardous for the safety and reliability of the transportation mission. Only during the phases when rotorcraft take off or land, the cable will run into slackness situation. A predefined formation can be used in those phases.

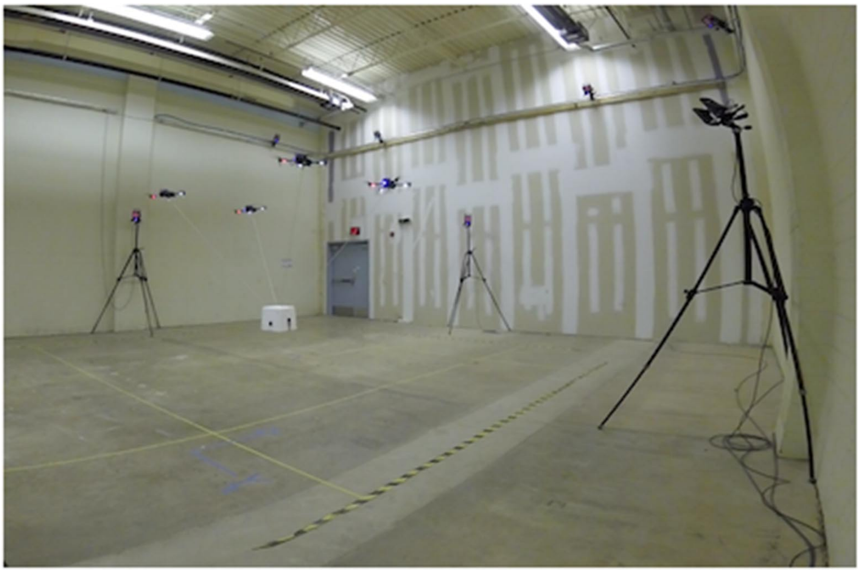

Fig. 3 Indoor flight of autonomous multilift [22,23].

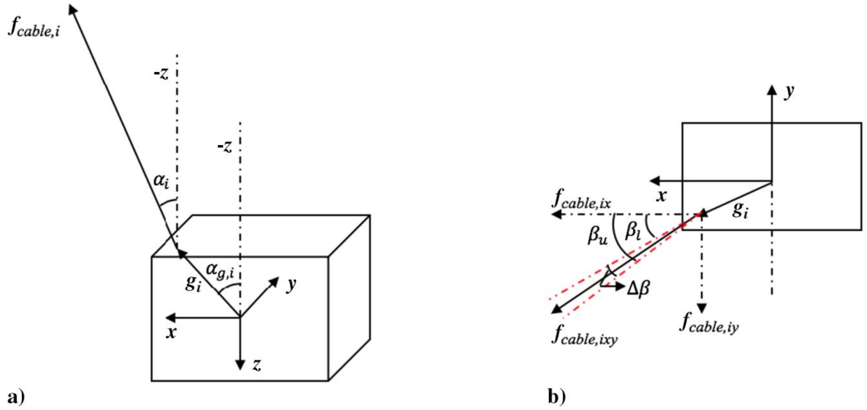

Fig. 4 Definition of cable cone angle and sector region.

the vertical axis of payload body frame is designed to be maintained at a specified value to ensure vehicle separation and payload controllability. In fact, it has been shown that the payload becomes more controllable as the cone angle increases [25]. However, it requires higher cable tension. Notice that here a fix cable cone angle case is considered since it is the scenario for most of cruise flight.

A. Trajectory Planning Problem

To equalize the load distribution, Berrios et al. designed a cost function to penalize the load distribution inequality of the tension difference between two cables [10] for a dual-lift system. A feedback controller was designed based on the difference in the cable tension error. However, increasing the number of rotorcraft beyond two adds complication. It is necessary to find a proper measure to quantify the load distribution. Here, minimizing the tension variance of all the cables is proposed so that the load distribution can be equalized. The control input or the cable force can also be planned at the same time.

Remark 1: For a near-hover payload with equal cable cone angles, the cable tension is directly related to the power of rotorcraft. By equalizing the cable tension, the rotorcraft can achieve near-evenly distributed power [9,10].

Let us consider the payload state vector $\boldsymbol{x} = [\boldsymbol{p}^T, \boldsymbol{\Omega}^T, \dot{\boldsymbol{p}}^T, \boldsymbol{\omega}^T]^T$, where $\boldsymbol{\omega}$ is payload angular rate in $\mathcal{F}_L$. The input vector is chosen as $\boldsymbol{u} = [T_1, \beta_1, T_2, \beta_2, T_3, \beta_3, T_4, \beta_4]^T$, where T_i is the tension magnitude of the ith cable, $i = 1, \ldots, 4$, and β_i is the angle between the cable force projection on the 2D plane (payload body x-y plane) and the positive direction of payload body x axis.

Hence, the trajectory planning problem based on load distribution can be formulated as

$$\begin{aligned} \min_{\boldsymbol{u}} \quad & J = \Phi(t_f) + \int_{t=t_0}^{t=t_f} L(\boldsymbol{x}, \boldsymbol{u})\, \mathrm{d}t \\ \text{subject to} \quad & \boldsymbol{x}(t_0) = \boldsymbol{x}_0 \\ & \boldsymbol{x}(t_f) = \boldsymbol{x}_{t_f} \\ & 0 \le T_i \le T_{\max}, \quad \beta_{il} \le \beta_i \le \beta_{iu}, \quad i = 1, \ldots, 4 \\ & |\phi| \le \phi_{\max}, \quad |\theta| \le \theta_{\max} \\ & \dot{\boldsymbol{x}} = f(\boldsymbol{x}, \boldsymbol{u}) \end{aligned} \tag{1}$$

where $\Phi(t_f) = 0$, $L(\boldsymbol{x}, \boldsymbol{u}) = (1/4) \sum_{i=1}^{4} [T_i - (1/4) \sum_{j=1}^{4} T_j]^2$ is the variance of the cable tension, $\boldsymbol{x}(t_0)$ and $\boldsymbol{x}(t_f)$ are the waypoints given before flight, $T_{\max}$ is the maximum tension cable can sustain, $\phi_{\max}$ and $\theta_{\max}$ are the payload small attitude limits, and $f(\cdot)$ is the payload equation of motion given by

$$\dot{\boldsymbol{x}}_L = \left[\dot{\boldsymbol{p}}^T, \dot{\boldsymbol{\Omega}}^T\right]^T \quad \text{(kinematics)} \tag{2}$$

$$\begin{aligned} m\ddot{\boldsymbol{p}} &= \sum_{i=1}^{4} \boldsymbol{R}_{L2e} \boldsymbol{f}_i + m\boldsymbol{g} \quad \text{(dynamics: Newton equation)} \\ \boldsymbol{J}\dot{\boldsymbol{\omega}} &= \sum_{i=1}^{4} \boldsymbol{g}_i \times \boldsymbol{f}_i - \boldsymbol{\omega} \times \boldsymbol{J}\boldsymbol{\omega} \quad \text{(dynamics: Euler equation)} \end{aligned} \tag{3}$$

where $\dot{\boldsymbol{\Omega}} = \boldsymbol{W}_L \boldsymbol{\omega}$, and

$$\boldsymbol{W}_L = \begin{bmatrix} 1 & \sin\phi\tan\theta & \cos\phi\tan\theta \\ 0 & \cos\phi & -\sin\phi \\ 0 & \sin\theta/\cos\theta & \cos\phi/\cos\theta \end{bmatrix} \tag{4}$$

m is payload mass, $\boldsymbol{J}$ is the payload inertia matrix with J_{xx}, J_{yy}, J_{zz} as the diagonal terms, $\boldsymbol{g}_i$ is the geometry vector from the payload center of mass (CM) to the ith cable attachment point in frame $\mathcal{F}_L$ (note overloaded use of $\boldsymbol{g}$; see Fig. 1b), and $\boldsymbol{f}_i = [T_i \sin\alpha\cos\beta_i, T_i\sin\alpha\sin\beta_i, -T_i\cos\alpha]^T$ is the ith cable force vector in frame $\mathcal{F}_L$.

Notice that in Eqs. (2) and (3), the angular motion is independent of translation motion. However, the translation motion is directly affected by the angular motion. The objective cost of Eq. (1) (i.e., the variance of cable tension) is in a quadratic form, and the system equations of motion are nonlinear.

B. Tracking Problem

Once the desired payload trajectory is generated, a feedback controller is designed for the system to track the desired reference trajectory.

Here, a small perturbation method linearizing the dynamic about the nominal path inspired by the classical neighboring feedback control approach is used [26]. Let us consider small perturbation from the desired nominal path. It is expected that such perturbations will give rise to perturbation $\delta\boldsymbol{x}$, $\delta\boldsymbol{u}$, governed by linearizing the system equations of motion (2) and (3) around the extremal path, $\delta\boldsymbol{x} = \boldsymbol{x}(t) - \boldsymbol{x}^*(t)$, $\delta\boldsymbol{u} = \boldsymbol{u}(t) - \boldsymbol{u}^*(t)$:

$$\begin{gathered} \delta\dot{\boldsymbol{x}} = f_x \delta\boldsymbol{x} + f_u \delta\boldsymbol{u} \\ \delta\boldsymbol{x}(t_0))\text{specified}, \quad \delta\boldsymbol{x}(t_f))\text{specified} \end{gathered} \tag{5}$$

where f_x and f_u are the Jacobian of Eq. (2) and (3) with respect to the nominal path. The system is supposed to track the desired trajectory, which means that the perturbations $\delta\boldsymbol{x}$ and $\delta\boldsymbol{u}$ should be small. The problem is formulated as finding control law of $\delta\boldsymbol{u}$ to minimize the energy due to perturbation:

$$\begin{aligned} \min_{\delta\boldsymbol{u}} \quad & \delta^2 J = \frac{1}{2}\int_{t_0}^{t_f}\left(\delta\boldsymbol{x}^T Q \delta\boldsymbol{x} + \delta\boldsymbol{u}^T R \delta\boldsymbol{u}\right) \\ \text{subject to} \quad & \delta\dot{\boldsymbol{x}} = f_x\delta\boldsymbol{x} + f_u\delta\boldsymbol{u} \\ & \delta\boldsymbol{x}(t_0))\text{specified}, \quad \delta\boldsymbol{x}(t_f))\text{specified} \end{aligned} \tag{6}$$

where Q and R are some positive definite matrices.

The overall control required to drive $\boldsymbol{x}(t_0) + \delta\boldsymbol{x}(t_0)$ to a final state would be equal to

$$\boldsymbol{u}(t) = \boldsymbol{u}^*(t) + \delta\boldsymbol{u}^*(t) \tag{7}$$

Notice that $\boldsymbol{u}^*(t)$ is the preplanned payload nominal input under given cable force constraints. Redundancy for real flight perturbation has already been considered in the constraints to guarantee the overall control $\boldsymbol{u}(t)$ still be within the system flight ability. In this regard, no designed constraints will be added on $\boldsymbol{u}(t)$.

III. Analysis and Methodology

A. Planning

1. Problem Analysis

The Hamiltonian of Eq. (1) can be defined as

$$H(\boldsymbol{x}, \boldsymbol{u}) = L(\boldsymbol{x}, \boldsymbol{u}) + \boldsymbol{\lambda}^T f(\boldsymbol{x}, \boldsymbol{u})$$

where $\boldsymbol{\lambda}$ defines the costates. The first-order necessary conditions for optimal trajectory with no active constraints are then given by $\dot{\boldsymbol{x}} = H_\lambda$, $\dot{\boldsymbol{\lambda}} = -H_{\boldsymbol{x}}$, and $H_{\boldsymbol{u}} = 0$, where the subscript means the gradient.

Remark 2: The Appendix describes the necessary conditions in detail. From these equations, it can be inferred that there is trivial solution for the costate vector $\boldsymbol{\lambda}$ when the cable tensions are equal, i.e., $(1/4)\sum_{i=1}^4 [T_i - (1/4)\sum_{j=1}^4 T_j]^2 = 0$. In fact, for the ideal case when all the cable tensions are equal,

$$L_{u_i} = \frac{3}{8}T_i - \frac{1}{8}\sum_{j\neq i} T_j = 0, \quad i, j = 1, 3, 5, 7$$

H_u can be written as a linear combination of the costates: $H_u = \boldsymbol{E}\tilde{\boldsymbol{\lambda}}$, where $\tilde{\boldsymbol{\lambda}} = [\lambda_7, \ldots, \lambda_{12}]^T$. It is easy to show that $\boldsymbol{E}$ has rank 6 under the setup in this problem. Hence, $\tilde{\boldsymbol{\lambda}} = 0$ for $H_u = 0$. Furthermore, Eqs. (A6) and (A10) corresponding to $\dot{\boldsymbol{\lambda}} = -H_x$ lead to $\lambda_k = 0$, $k = 1, 2, 3$, when $\tilde{\lambda} = 0$. Similarly, Eqs. (A7) and (A11–A13) lead to $\lambda_4 = \lambda_5 = \lambda_6 = 0$.

Note that zero costate implies that H_u, H_{uu}, and higher-order derivatives are all zero. Physically, it implies that payload dynamics do not affect the solution. Intuitively, this means that one can always find an equal tension solution, as long as the system is near-hover (i.e., acceleration is small and external forces such as drag are small). For a fixed cone angle, equal cable tension implies five unknowns of input (tension and four sector angles), and payload dynamics includes six equations. Hence, there is a least-squares solution for a specified acceleration. However, for large acceleration or large external force (aerodynamic drag), cable angle constraints will become active, and that may make an equal tension solution impossible.

2. Collocation

A variety of methods have been developed to solve this nonlinear trajectory optimization problems [27,28]. Here, the direct collocation method is used, converting the trajectory optimization problem into a nonlinear programming problem [29].

According to this method, the time is first discretized into N uniformly distributed subintervals (for the fixed final time case). Then, an initial guess of states and input for each one of the $N+1$ collocation points $\bar{\boldsymbol{x}}(t_k)$, $\bar{\boldsymbol{u}}(t_k)$, $k = 1, \ldots, N$, is given. In each interval, since $\dot{\bar{\boldsymbol{x}}}(t_k)$ can also be obtained through the system dynamics, a cubic interpolation for states while linear interpolation for inputs can be performed. Denote $\tau = (t - t_k/h)$, where $h = t_k - t_{k-1}$.

$$\begin{aligned} x_i^k(\tau) &= a_i^k + b_i^k\tau + c_i^k\tau^2 + d_i^k\tau^3 \\ \dot{x}_i^k(\tau) &= \frac{b_i^k}{h} + 2\frac{c_i^k\tau}{h} + 3\frac{d_i^k\tau^2}{h} \\ u_i(\tau) &= \bar{\boldsymbol{u}}_i(t_k) + \left(\bar{\boldsymbol{u}}_i(t_{k+1}) - \bar{\boldsymbol{u}}_i(t_k)\right)\tau \end{aligned}$$

where the subscripts i, j denote the ith states and jth input, and $x_i^k(0) = \bar{\boldsymbol{x}}_i(t_k)$, $x_i^k(1) = \bar{\boldsymbol{x}}_i(t_{k+1})$, $\dot{x}_i^k(0) = f_i(\bar{\boldsymbol{x}}(t_k), \bar{\boldsymbol{u}}(t_k))$, and $\dot{x}_i^k(1) = f_i(\bar{\boldsymbol{x}}(t_{k+1}), \bar{\boldsymbol{u}}(t_{k+1}))$. The midpoint of each interval can then be evaluated easily as well as the error:

$$\begin{aligned} x_i^k(1/2) &= \frac{1}{2}\left(\bar{\boldsymbol{x}}_i(t_k) + \bar{\boldsymbol{x}}_i(t_{k+1})\right) \\ &\quad + \frac{h}{8}\left[f_i\left(\bar{\boldsymbol{x}}(t_k), \bar{\boldsymbol{u}}(t_k)\right) - f_i\left(\bar{\boldsymbol{x}}(t_{k+1}), \bar{\boldsymbol{u}}(t_{k+1})\right)\right] \\ \dot{x}_i^k(1/2) &= -\frac{3}{2h}\left(\bar{\boldsymbol{x}}_i(t_k) - \bar{\boldsymbol{x}}_i(t_{k+1})\right) \\ &\quad - \frac{1}{4}\left[f_i\left(\bar{\boldsymbol{x}}(t_k), \bar{\boldsymbol{u}}(t_k)\right) + f_i\left(\bar{\boldsymbol{x}}(t_{k+1}), \bar{\boldsymbol{u}}(t_{k+1})\right)\right] \\ u_i^k(1/2) &= \frac{\bar{\boldsymbol{u}}_i(t_k) + \bar{\boldsymbol{u}}_i(t_{k+1})}{2} \end{aligned}$$

By evaluating the error,

$$e_i^k = \dot{x}_i(1/2) - f_i\left(\bar{\boldsymbol{x}}(t_{k+(h/2)}), \bar{\boldsymbol{u}}(t_{k+(h/2)})\right)$$

The original optimal control problem thus is transcribed as a nonlinear programming problem

$$\min_{\boldsymbol{u}} \quad J = \Phi(\boldsymbol{x}(t_N)) + \frac{1}{2}\sum_{k=0}^{N}\Big[L\Big(\bar{\boldsymbol{x}}(t_k), \bar{\boldsymbol{u}}(t_k), t_k\Big) + L\Big(\bar{\boldsymbol{x}}(t_{k+1}), \bar{\boldsymbol{u}}(t_{k+1}), t_{k+1}\Big)\Big]h \tag{8}$$

$$\text{subject to} \quad e_i^k = 0, \quad k = 0, 1, 2, \ldots, N \tag{9}$$

B. Tracking

Problem (6) is a linear quadratic problem. Analytic solution can be obtained by using Bryson's backward sweep method [26].

$$\begin{aligned}\delta\boldsymbol{u}(t) &= -(K - R^{-1}B^T V P^{-1} V^T)\delta\boldsymbol{x}(t) \\ &= -R^{-1}B^T V P^{-1}\delta\boldsymbol{x}(t_f)\end{aligned} \tag{10}$$

where

$$A(t) = f_x, \quad B(t) = f_u \tag{11}$$

$$\begin{aligned}-\dot{S} &= A^T S + SA - SBR^{-1}B^T S + Q \\ K &= R^{-1}B^T S \\ -\dot{V} &= (A - BK)^T V \\ \dot{P} &= V^T B R^{-1} B^T V\end{aligned} \tag{12}$$

where $S(t_f) = 0$ is given, $V(t_f) = I$, and $P(t_f) = 0$. Notice that the feedback control term $\delta\boldsymbol{u}$ only relies on the state error, which means that there is no need to put on cable tension sensors along the cables.

IV. Simulation

In this section, numerical simulation results are presented. Three test cases are considered for planning: one with the given final time $t_f = 5.0$ s based on the flight tests described in [22,23], and the other two with $t_f = 2.8$ and 2.3 s by reducing the arriving time to stress the system. As for the tracking, the system is simulated by applying the designed neighboring feedback controller (11) under the wind gust environment to show the effectiveness of the developed feedback controller.

A. Setup

1. Multilift Parameter

Remember that the system is treated as a rigid-body motion with a set of cable forces as inputs based on the assumption that the rotorcraft can respond instantly to commands for some bounded set of cable forces. Therefore, the simulation model is the payload 6D equation of motion; see (2) and (3) with the planned cable forces as the inputs. Tables 1 and 2 list all of the parameters for payload and cables as well as the cable attachment geometry; see also [22].

Table 1 Parameter for payload and cables

Parameter	Value
Cable length	2.1 m
Payload length	0.3525 m
Payload width	0.298 m
Payload height	0.325 m
$T_{\max}$	4.5 N
Cone angle α	37.0 deg
Payload weight	0.815 kg
Payload I_x	0.0170 $\mathrm{kg \cdot m^2}$
Payload I_y	0.0287 $\mathrm{kg \cdot m^2}$
Payload I_z	0.0106 $\mathrm{kg \cdot m^2}$
Sector region $\Delta\beta$	30 deg
Sector center β_c	35.2 deg

Table 2 Cable attachment geometry

Attachment no.	g_x, m	g_y, m	g_z, m
1	0.115	−0.090	−0.203
2	0.115	0.090	−0.203
3	−0.115	0.090	−0.203
4	−0.115	−0.090	−0.203

2. Setup for Trajectory Planning

For the trajectory planning problem, the system is scheduled to fly from waypoint A to B. Without loss of generality, pick A as the origin with zero velocity and payload level. B is a waypoint with prescribed position $\boldsymbol{p}_B = [1.5, 1.8, -0.9]^T$ and zero velocity and payload level.

The nonlinear programming solver "fmincon" in MATLAB is used to solve Eq. (8). The "sqp" algorithm (sequential quadratic programming) is selected. After some trial computations, $Np = 31$ collocation points are used to balance computation speed and accuracy.

The polynomial curve method described in [22,23] is used for generating an initial guess of the payload states $\boldsymbol{x}$. The trajectory is generated from a third-order polynomials as the linear and angular acceleration with zero boundary conditions. The payload linear and angular velocity and position are then generated by higher-order polynomials that satisfy waypoint boundary conditions. The total force and moment acting on the payload can then be obtained from the corresponding acceleration. Cable force as the payload input $\boldsymbol{u}$ is then initialized with least-norm solution to satisfy the net forces and moments and null space solution to satisfy cable tension magnitude and geometry constraints.

3. Tracking Controller Parameter

The parameters for the tracking controller are designed as $Q = 1.0 \times \boldsymbol{I}_{12\times 12}$ and $R = 3.0 \times \boldsymbol{I}_{8\times 8}$. Sweep method is then implemented to compute the controller gain (11). $\delta\boldsymbol{x}(t_0)$ is selected as a Gaussian random variable with zero mean and 6 cm position standard deviation based on the hardware flight test [22,23]. $\delta\boldsymbol{x}(t_f)$ is generated as a zero vector.

4. Wind Gust

Wind gusts is added as an external disturbance when the system is simulated during flight tracking the reference trajectory. This gust acts upon the payload as an aerodynamic drag force:

$$\boldsymbol{D} = \frac{1}{2}\rho \boldsymbol{v}_a^2 S C_d \tag{13}$$

where $\rho = 1.225\ \mathrm{kg/m^3}$ is the air density, $\boldsymbol{v}_a$ is payload airspeed, S is the reference area of payload, and C_d is the drag coefficient. A mild wind gust $\boldsymbol{w}$ modeled using a normal distribution with zero mean and standard deviation 2.5 m/s is considered. Also, notice that the inertial speed of payload $\boldsymbol{v} = \boldsymbol{v}_a + \boldsymbol{w}$.

B. Planning Results and Discussion

Figure 5 shows the payload states of all three cases. It can be seen that the nonlinear solver can find the minimum that satisfies all the constraints. The payload is able to be driven to the destination for all cases.

Note that the position and velocity histories of the polynomial trajectory and the optimal (i.e., load-distributed) solution are very close. Orientation and angular rate, however, differ significantly. The reason for this lies in the mechanism for payload motion under load-distribution control: translation occurs via changes in payload orientation (similar to translation control of a multirotor).

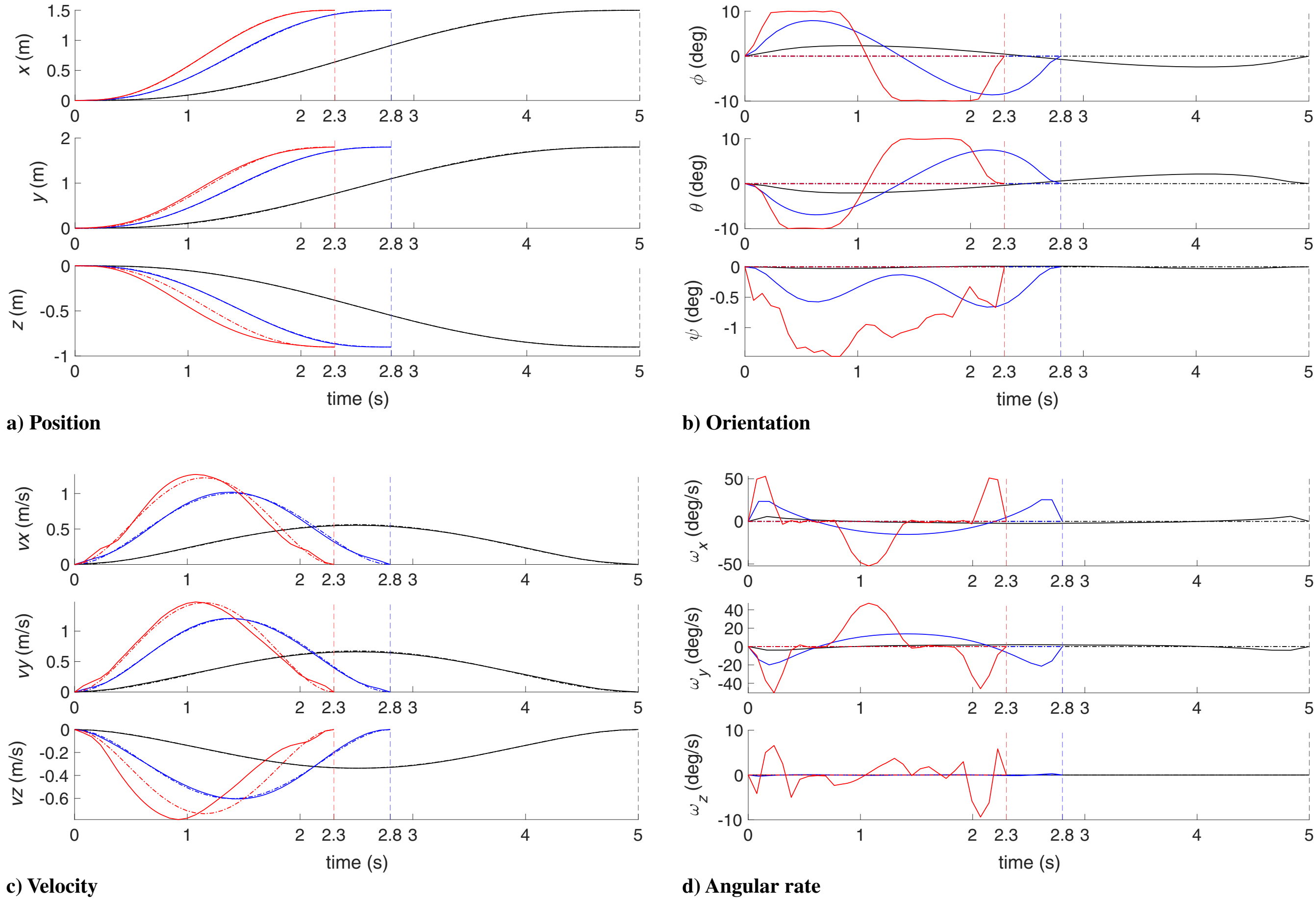

Fig. 5 Payload state for $t_f = 5.0$ (black), 2.8 (blue), and 2.3 (red) s: initial guess (dashed) and optimal solution (solid).

The initial and optimized cable tension as well as the sector angle of the four cables are compared in Figs. 6 and 7. Note that the cable tensions along each tether resulting from the optimal load distribution controller are very nearly equal distributed throughout the payload trajectory.

From Figs. 5, 6b, and 7b, one can observe by reducing the arriving time that all the cable tension increases but still with a evenly distributed load. The payload ended with a larger rotation maneuver and a more aggressive change of sector angle in order to achieve the goal in a shorter time by bigger acceleration. If reducing the arriving time even further, see the case when $t_f = 2.3$ s (Figs. 5b, 6c, and 7c); in order to achieve the goal while maintaining small attitude, the system can only accelerate by changing the sector angle, resulting in hitting the bound with a heavy fluctuation, which (depending on the payload contents) may not be ideal. Therefore, one can say that this mission cannot be achieved by small maneuver.

Remark 3: In general, the solution obtained from the direct method is only a numerical local minimum. However, in the problem discussed above, the direct collocation method can find the optimal solution (i.e., equal cable tension) for near hover situation (small maneuver).

As a rank check, the singular value of the costate coefficient matrix $\boldsymbol{E}$ in Eq. (A3) has been computed and sorted from maximum to minimum. Figure 8 shows the ratio of the sixth singular value (minimum) over the first one (maximum) σ_6/σ_1 for all three cases. It validates that the rank of $\boldsymbol{E}$ is always 6 under the planned trajectories. Furthermore, in the optimal situation under equal cable tension, the necessary condition (A1) and the rank of $\boldsymbol{E}$ indicate zero costates. Physically, this means that one can always find an equal tension solution under the small maneuver.

C. Tracking Results Under Wind Gust

Figure 9 shows the tracking error when $t_f = 5.0$ and 2.8 s for both initial polynomial trajectory and optimal load-distribution trajectory. The system encounters disturbance during the flight under the wind gust environment. The feedback controller is able to correct the system and drive the slung load to the desired trajectory.

As for the control input, Fig. 10 shows the input tracking error for optimal trajectory tracking. None of the inputs saturates during the flight simulation. However, the case when $t_f = 2.8$ s clearly shows a bigger tracking error due to the bigger maneuver. Table 3 shows the maximum cable tension tracking error for both the initial and optimal trajectory tracking. The initial trajectory tracking ends with a bigger cable tension tracking error, which is harmful for the real hardware flight because the overload due to the uneven distributed tension could cause motor and power failure for the vehicle with the highest cable tension.

Table 4 shows the load distribution cost, or the total cable tension variance of four groups of trajectory: initial guess, optimized trajectory, and flight simulation under wind gust for two cases. Compared with the initial guess (i.e., the polynomial-derived trajectory), even with external disturbances (e.g., wind gusts) cable forces of the optimized trajectory are more evenly distributed. In fact, the cable load cost is still several orders of magnitude lower than the initial guess, even with wind gusts acting upon the payload.

V. Hardware Experiment

In this section, hardware flight tests in an indoor motion capture studio flight are performed to validate the proposed trajectory planning and control approaches.

A. Hardware Platform

The hardware implementation of a four rotorcraft multilift is described in detail in [22]. Major parts of the hardware platform are summarized here.

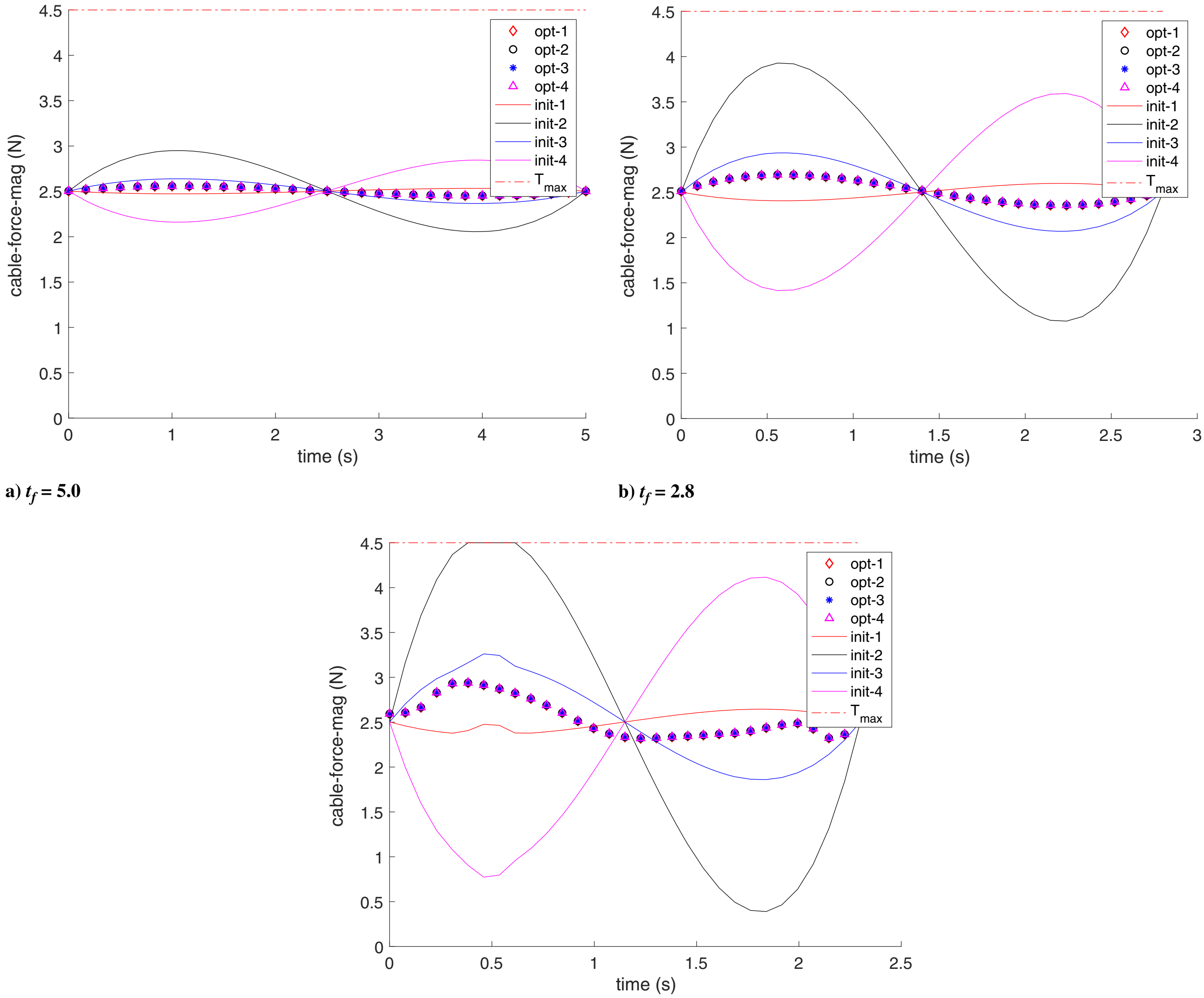

a) $t_f = 5.0$

b) $t_f = 2.8$

c) $t_f = 2.3$

Fig. 6 Cable tension.

1. Payload Side

A foam box with an ODroid-XU4, Pixhawk Mini autopilot, GPS +compass, and corresponding power supply inside perform as the payload, as shown in Fig. 11.

ODroid-XU4 is the onboard mission computer. A Python State Machine hosted on the XU4 manages the mission stages, conducts the payload trajectory controller, and performs the cable force computation. A WiFi adapter mounted on one of the USB ports of the ODroid is the communication tool. The Pixhawk Mini with a GPS +compass group connected communicates with the ODroid to provide payload real-time information (position, orientation, velocity, angular rate, acceleration). For indoor flight tests, a Vicon motion capture system provides position and orientation; during outdoor tests, payload position is provided by GPS. Four cable cords are attached to the payload.

2. Rotorcraft Side

Four 3DR IRIS quadcopters are the executors following the payload commands. The low-level control interface is a Pixhawk 1 autopilot with firmware PX4, which also provides access to the servo motors, barometric altimeter, and accelerometer, gyroscope, and magnetometer suite. On top of each IRIS, an ODroid-XU4 acts as a mission computer, communicating with the payload over ROS via WiFi. It also runs the high-level control and connects to the low-level interface (Pixhawk 1) through serial mavros.[¶]

3. Ground Side

A Xbox video gamepad connected to the ground laptop performs as the human interface, which can trigger different system flight states and also be responsible for starting safety mode. For the indoor flight, a Vicon machine also connected to the ground laptop receives real-time flight data and cast them into ROS space.

4. Information Flow

The information flow of the whole multilift system is shown in Fig. 12. The payload commands computed desired position, velocity, and acceleration to each rotorcraft so that the motion of rotorcraft can steer the payload to the desired states. Here, the payload states are position, orientation, velocity, and body rates. The ground station with a gamepad connected casts the human-interactive command to the payload. The navigation system, either Vicon or GPS, provides the position and velocity information for the payload.

[¶]Mavros Pacakge Summary, http://wiki.ros.org/mavros.

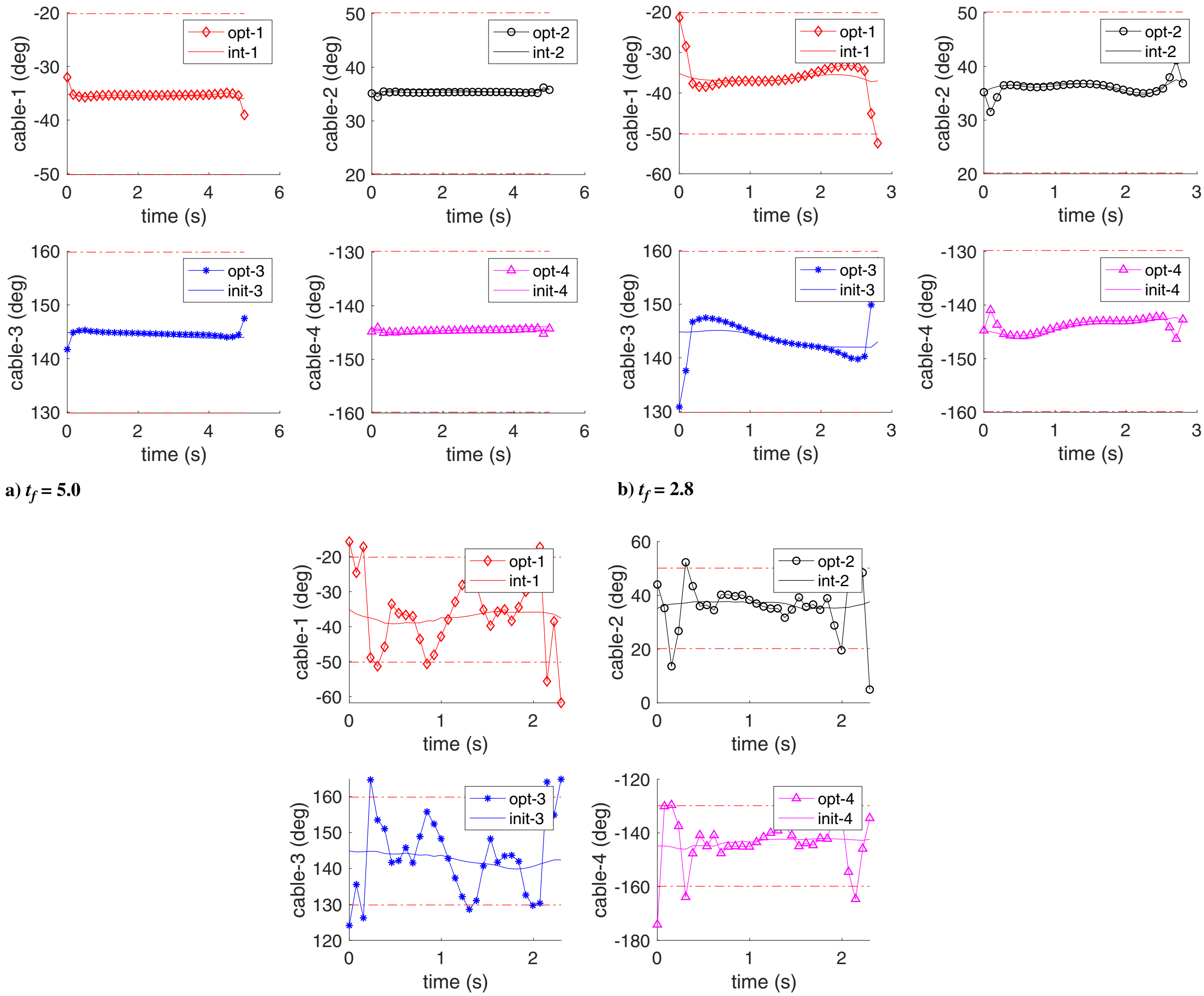

a) $t_f = 5.0$

b) $t_f = 2.8$

c) $t_f = 2.3$

Fig. 7 Cable sector angle.

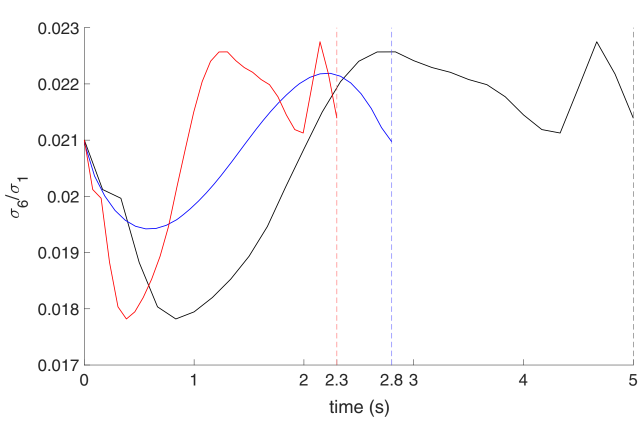

Fig. 8 The ratio of the sixth singular value over the first singular value of E for $t_f = 5.0$ (black), 2.8 (blue), and 2.3 (red) s.

All of the IRIS ODroids, the payload ODroid, and the ground laptop run in the same ROS space under the same WiFi network. The operator can remotely log into the onboard computer of either rotorcraft or payload from the ground laptop to launch the mission or monitor the performance of each individual object.

B. Experiment Implementation

The state machine includes five basic states: GROUND, TAKE_-OFF, HOVER, FOLLOW_TRAJ, and LANDING [22].

For the indoor flight tests, the whole system starts from the GROUND state. Once the ready switch is triggered, four rotorcraft fly to the takeoff position. Notice that the takeoff position is the one where the cables stretch to the equilibrium length so that the payload is still static but just about leaving the ground. It also makes the cables satisfy cone constraints and vehicle separation requirement.

The system will transit to HOVER then FOLLOW_TRAJ state to track some preplanned trajectories. In this paper, we plan the trajectory offline using the proposed approach based on load distribution. Then, the neighboring feedback controller runs onboard the payload to perform real-time tracking.

LANDING state will start when the payload arrives at the final desired states in the FOLLOW_TRAJ. All of the rotorcraft then descend to touch down on the ground.

C. Experiment Setup

The system is scheduled to lift off the ground for 0.5 m after takeoff in the FOLLOW_TRAJ state (denote this point as start point $A = [x_0, y_0, z_0]^T$); then fly to waypoint $B = [x_0 + 1.5, y_0 + 1.8, z_0 - 0.9]$ in 5.0 s; hold for 0.5 s and then fly back to A in 5.0 s; finally descend to touchdown and land. This design ensures that the system can be better

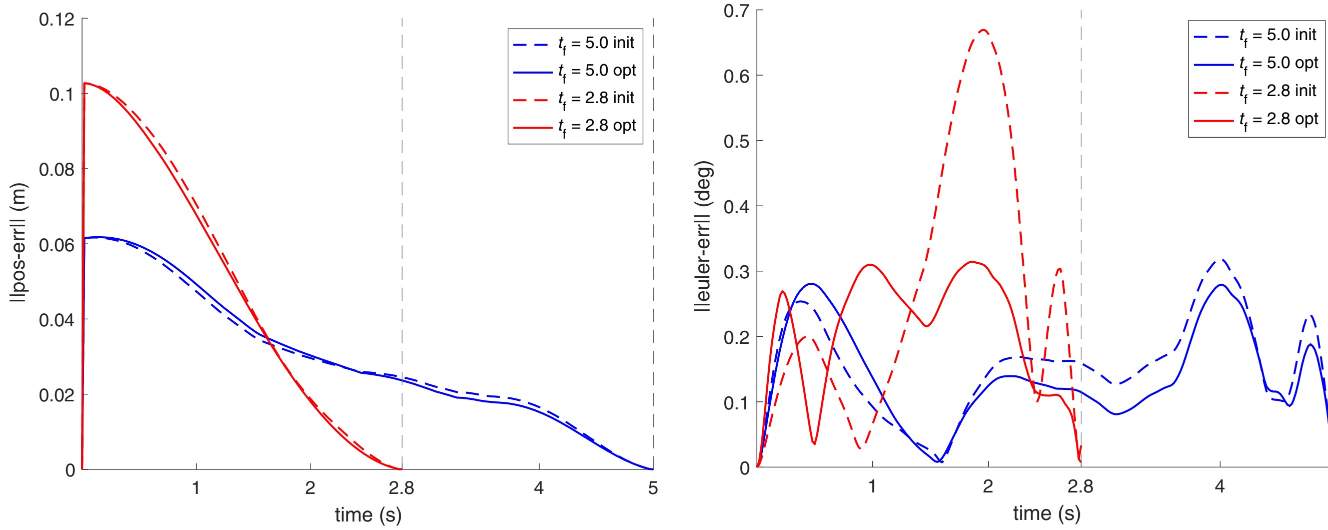

a) Position

b) Orientation

Fig. 9 Tracking error (in 2-norm) of payload states under wind gust.

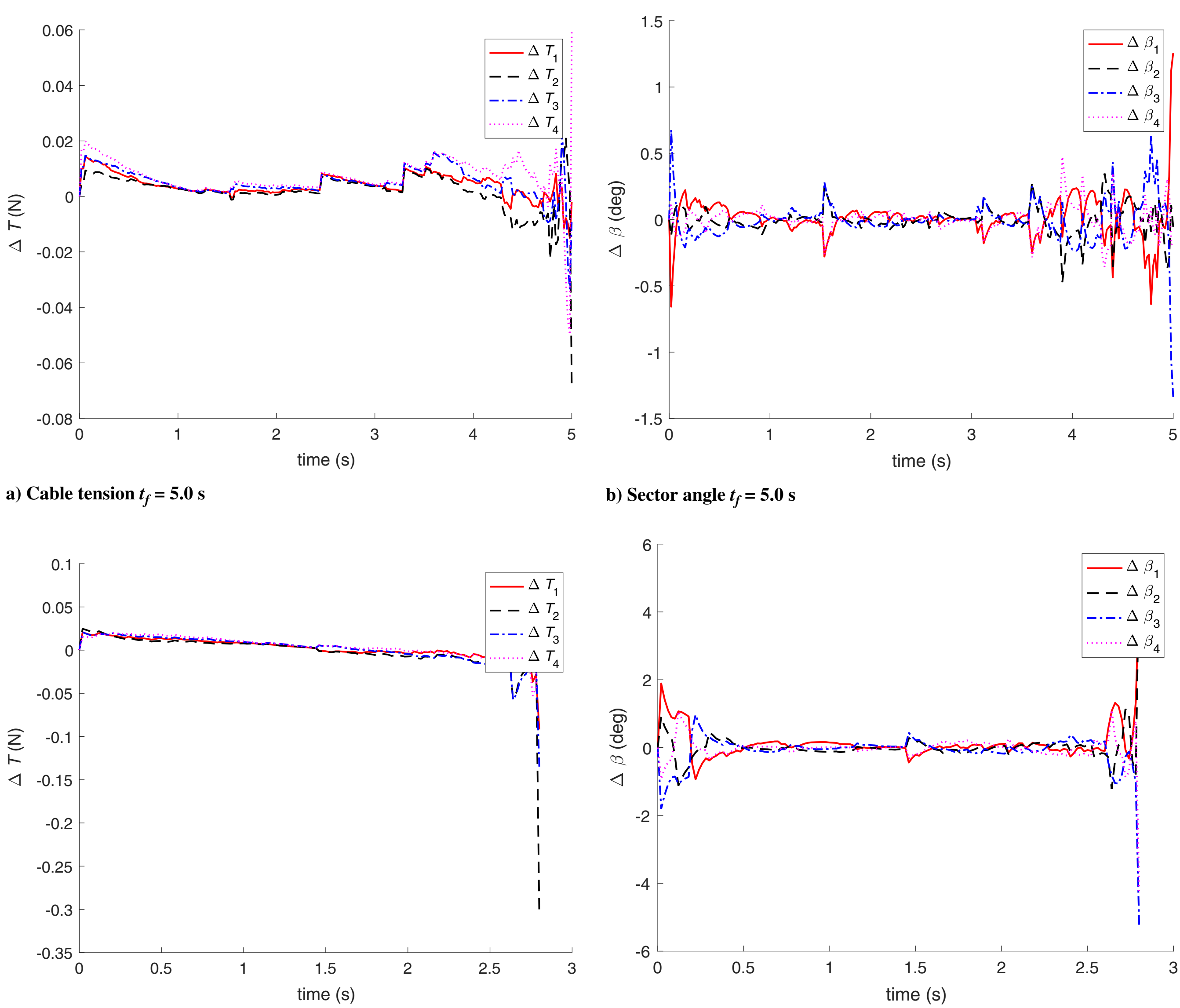

a) Cable tension $t_f = 5.0$ s

b) Sector angle $t_f = 5.0$ s

c) Cable tension $t_f = 2.8$ s

d) Sector angle $t_f = 2.8$ s

Fig. 10 Input tracking error.

Table 3 Maximum cable tension tracking error

Case	$t_f = 5.0$ s, N	$t_f = 2.8$ s, N
Initial trajectory	0.0821	0.1012
Optimized trajectory	0.0596	0.0893

Table 4 Cost of load distribution

	cost	
Case	$t_f = 5.0$ s, N^2	$t_f = 2.8$ s, N^2
Initial guess	13.8729	78.9977
Optimized trajectory	2.3731e − 09	2.6821e − 09
Initial trajectory tracking	14.0180	79.2331
Optimal trajectory tracking	0.0075	0.0337

fit in and use the available Vicon capture volume. Meanwhile, the system movement in all directions can be excited within the limitations of sensors and actuators.

The control parameters designed in simulation provide a start for real hardware flight. The final parameters used for the flight tests are the results after tweaking based on the Bryson's rule [26]. The basic idea of this technique is to normalize the effect that the state outputs and the control term may have on the quadratic cost function. The anticipated maximum values or deviation of the individual outputs and controls is usually used to accomplish this normalization, i.e.,

$$q_{ii} = \frac{1}{\max(x_i)^2}, \qquad i = 1, 2, \ldots, 12 \tag{14}$$

$$r_{jj} = \frac{1}{\max(u_j)^2}, \qquad j = 1, 2, \ldots, 8 \tag{15}$$

where q_{ii} is the ith diagonal component of matrix Q, r_{jj} is the jth diagonal component of matrix R, x_i is the ith components of $\boldsymbol{x}$, and u_j are the jth components of $\boldsymbol{u}$. The final parameters used in real hardware implementation are given in the Appendix.

Two cases are tested and compared: case 1, which uses the load-distribution-based planning and the neighboring feedback control approach proposed in this paper; case 2, which uses the polynomial curve planning method and the hierarchical approach with real-time cable force computation.

Fig. 12 Multilift system information flow.

D. Results and Discussion

Figure 13 depicts a sequence of images from the flight test. The system lifts the payload above the ground for 0.5 m at point A (Fig. 13a); on the way of flying to waypoint B (Fig. 13b); arrives waypoint B (Fig. 13c); and flies back to waypoint A.

Payload tracking performance is shown in Fig. 14. It can be seen that in both cases the payload can be transported to the desired waypoints successfully under the payload leading approach.

However, the cable tension and sector angle comparison presented in Figs. 15 and 16 show that the cable tension ends with a larger variance in case 2. Planning based on load distribution clearly reduced the cable tension variance by conducting proper feedback control. In fact, the cable sector angles are shown in Fig. 16. All cables remain in the valid quadrant with respect to the payload during flight within several degrees variation.

Figure 17 shows the four rotorcraft tracking performance. In both cases, the rotorcraft behaving as the actuators can effectively execute the payload command and track the commanded position.

Particularly, it is worth to notice that, due to the less variant cable tension performance, case 1 shows a superior power consumption performance. The power of each individual robot is measured using the voltage and current sensor reading from the battery. Then, at each timestamp, the total power is the summation of the power from each individual robot while the standard deviation quantifies the variation of the power consumption among each robot. Finally, the average total power or standard deviation is obtained by taking the average among the time history. In fact, Figs. 18a and 18b show the time history of the total power consumption and the standard deviation (std) of the power consumption of four rotorcraft. Table 5 provides a

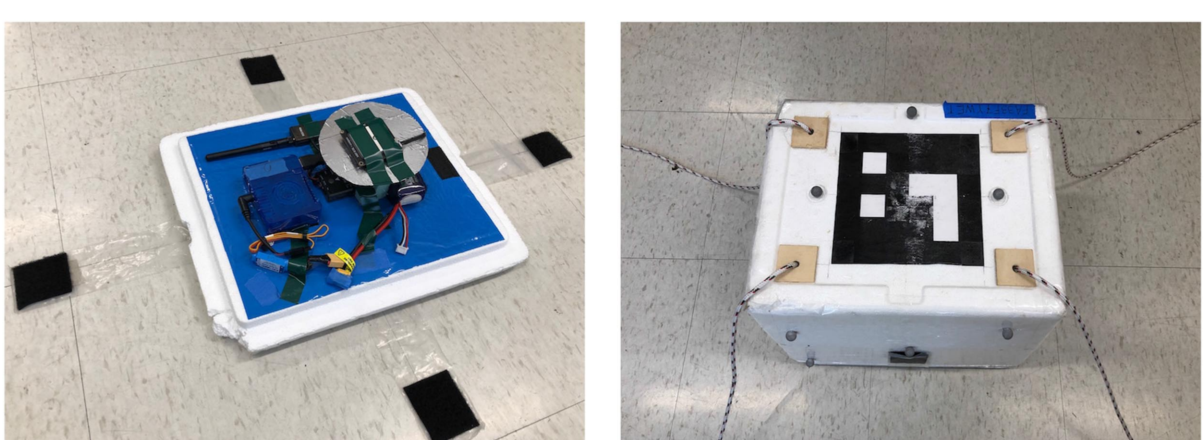

a) b)

Fig. 11 Payload with control computer.

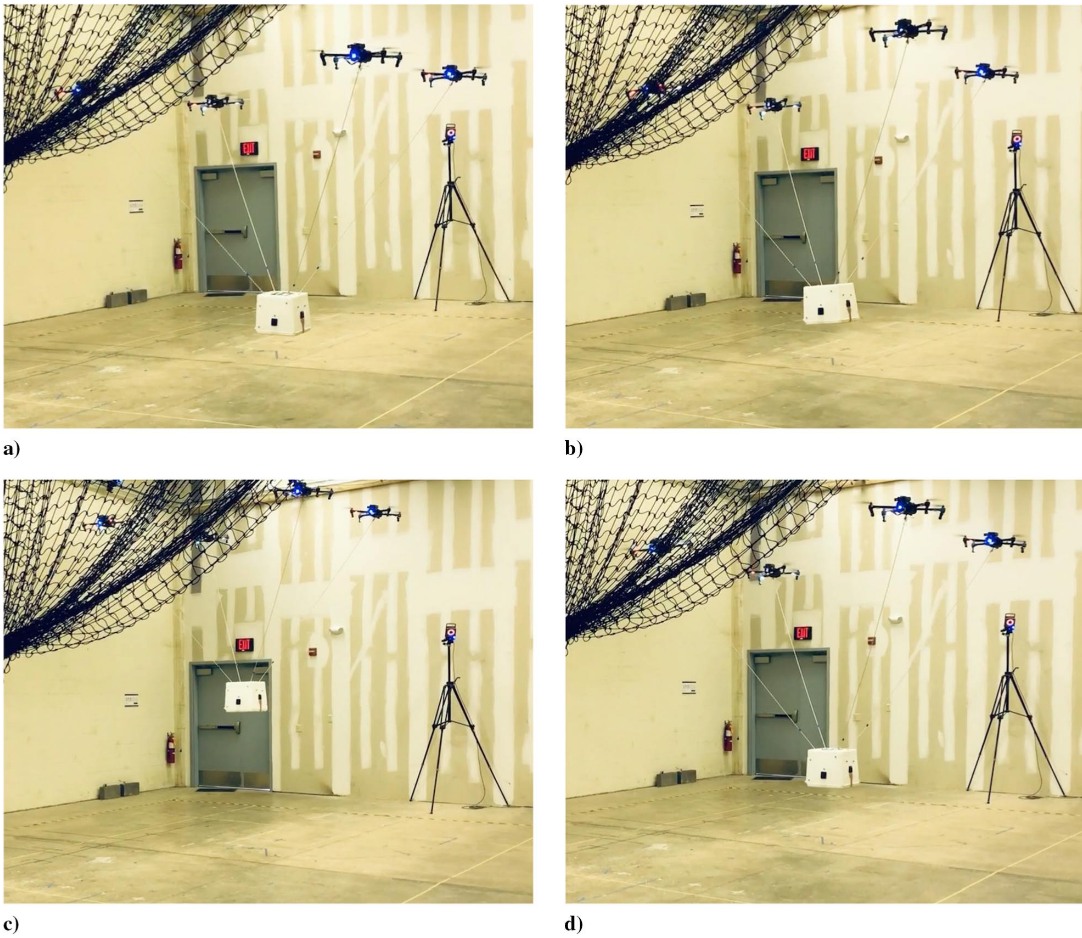

Fig. 13 Sequence of images showing system behavior using the proposed approach.

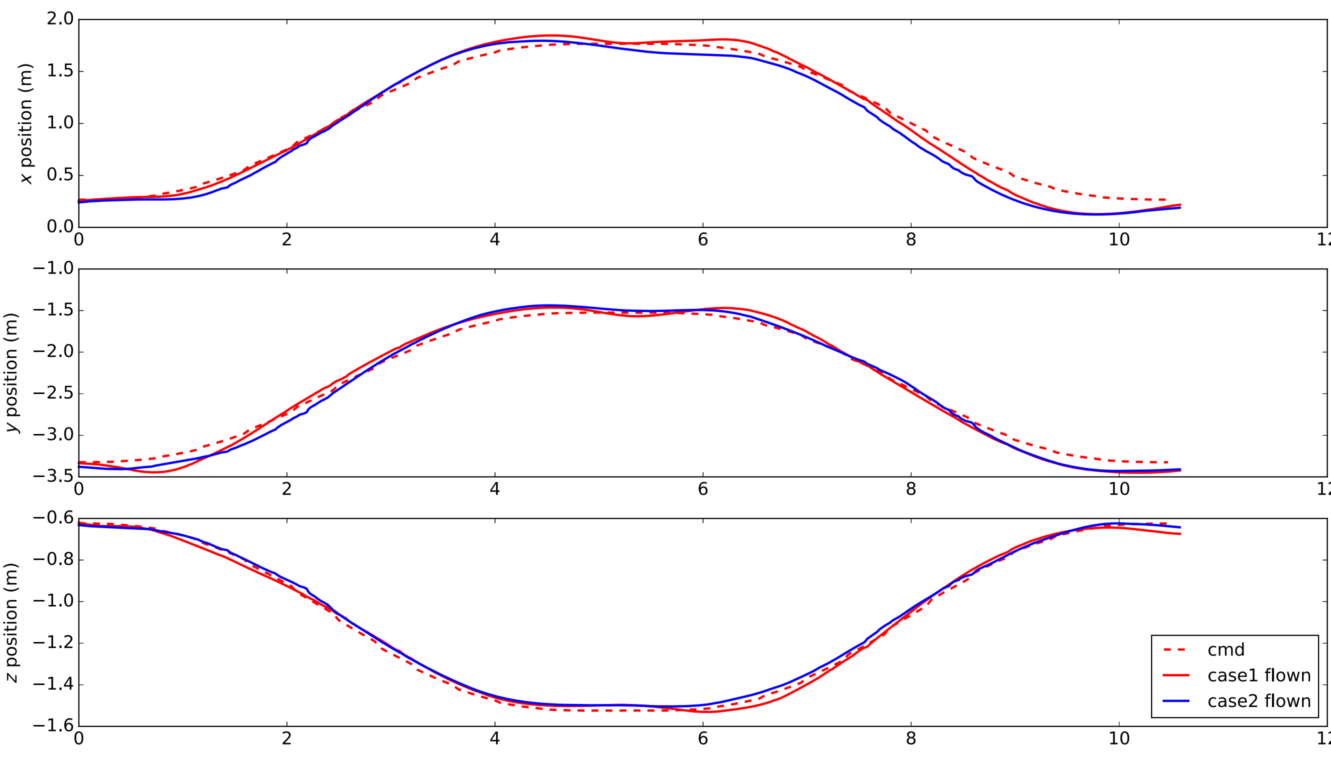

Fig. 14 Payload tracking performance.

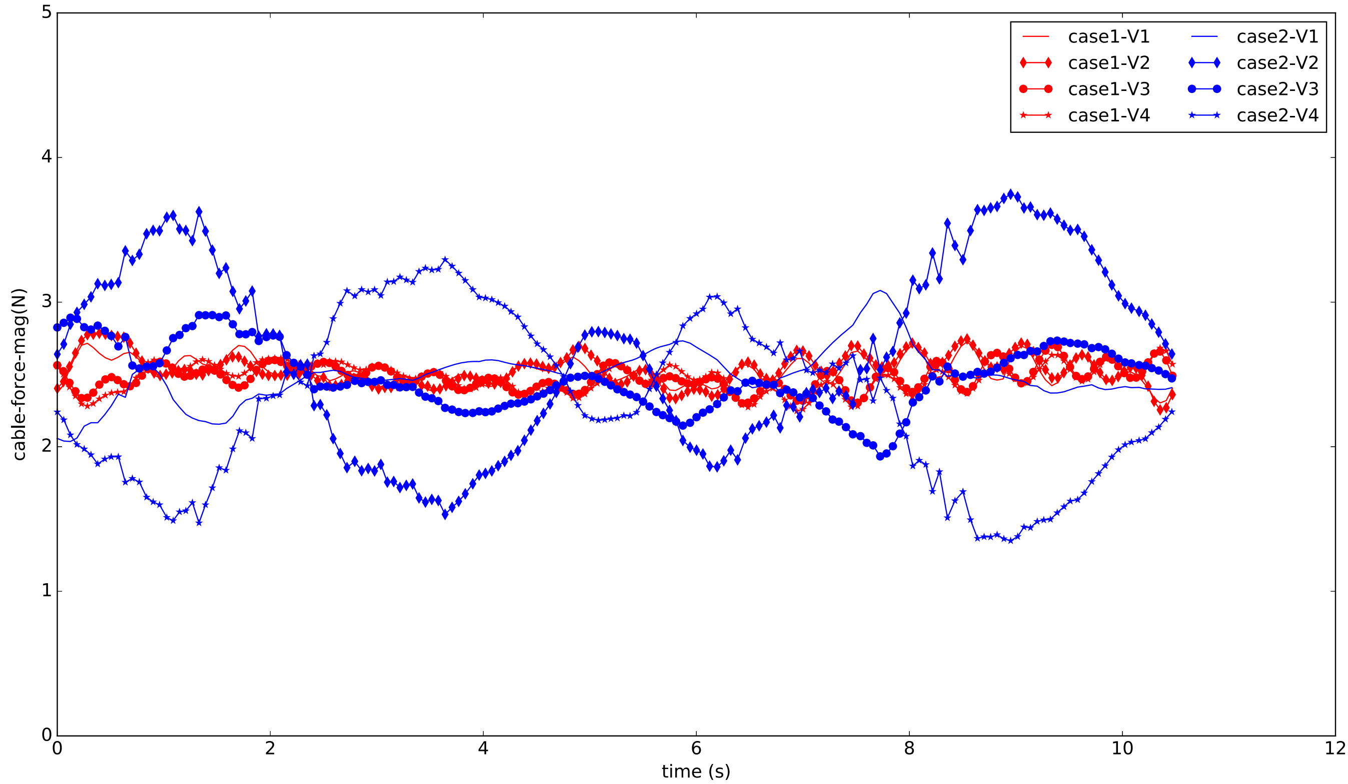

Fig. 15 Cable tension.

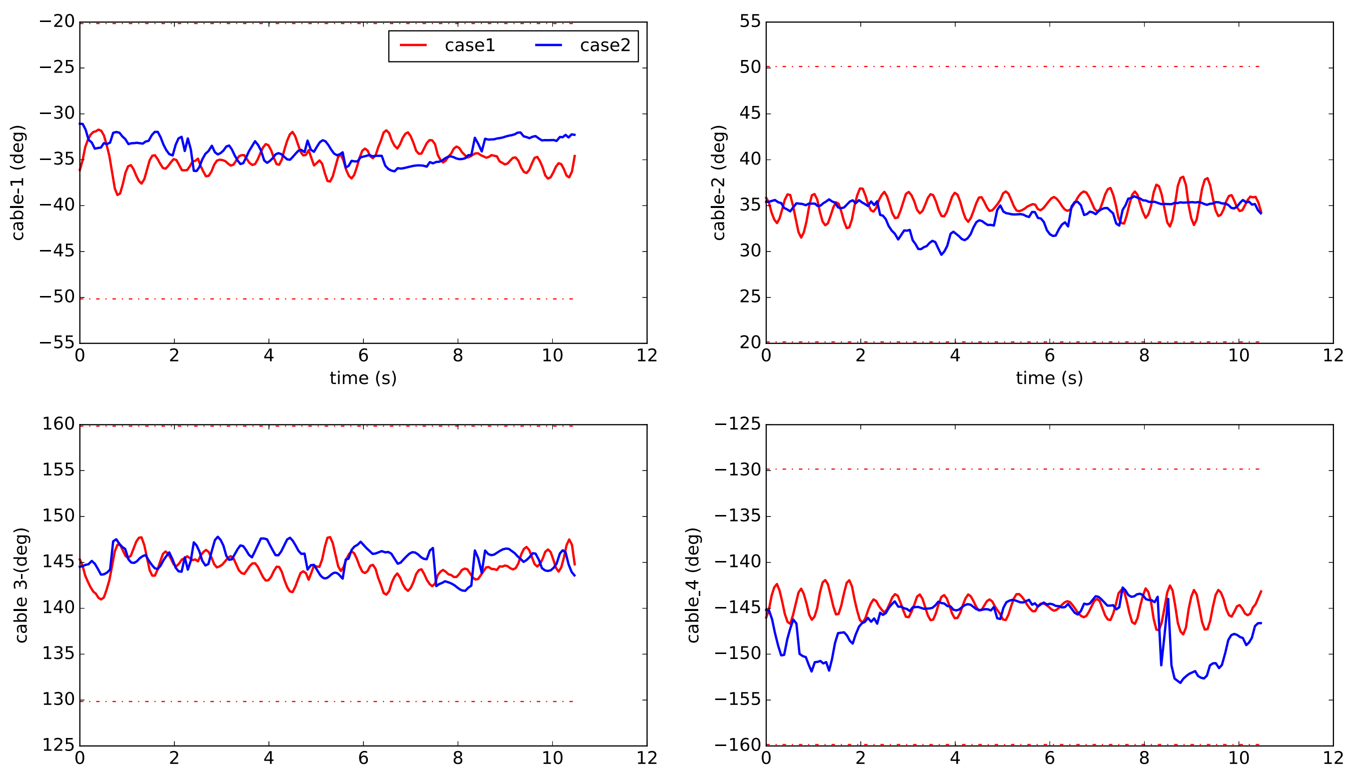

Fig. 16 Cable sector angle.

comparison of some specific quantities of the energy consumption performance. One can clearly observe that planning based on load distribution followed by the neighboring feedback control approach reduces the total power of the four robots. The multilift system achieves a more near-equal power consumption among the robots compared to the case without planning based on load distribution.

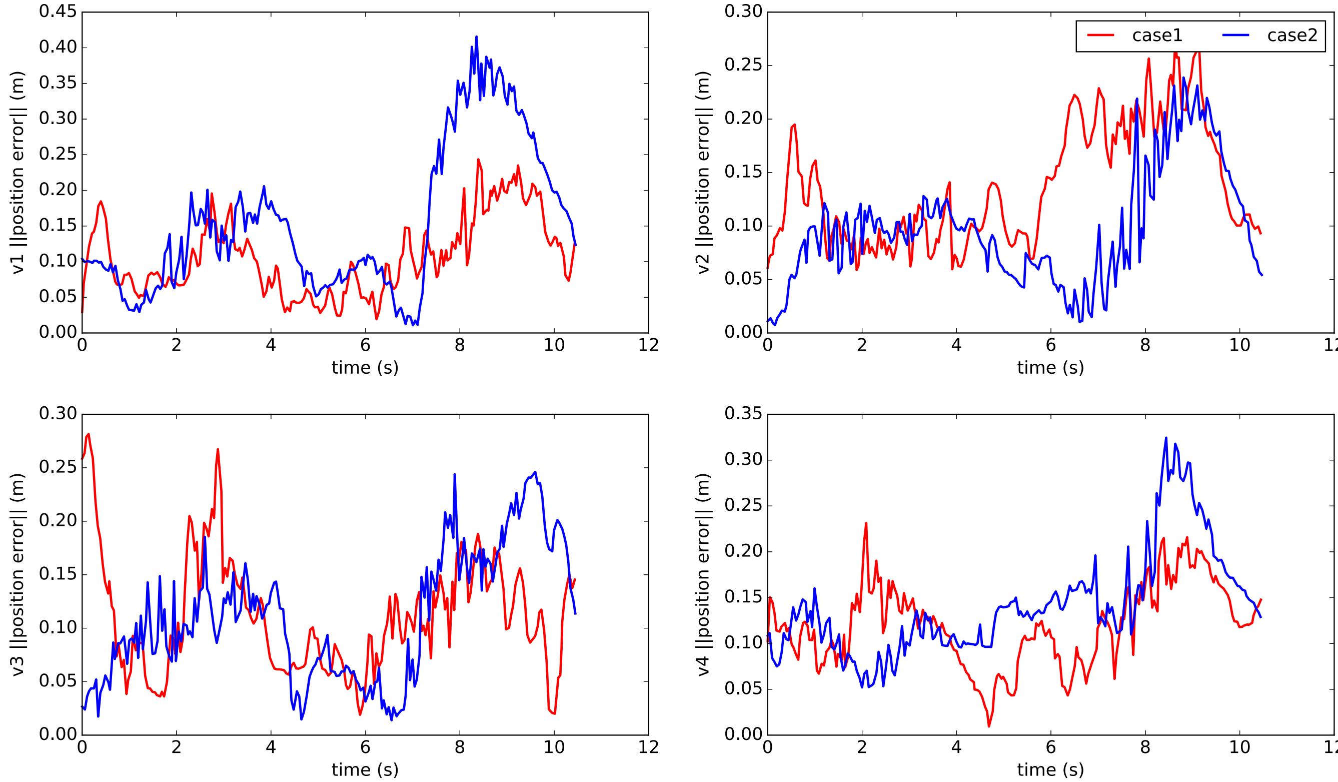

Fig. 17 Robots tracking performance.

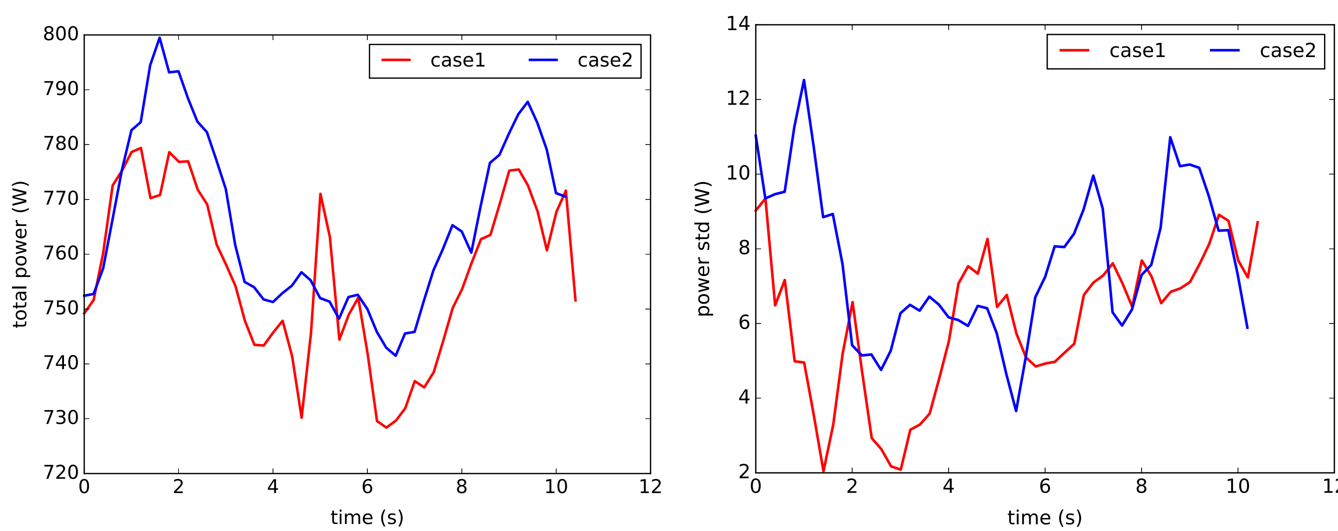

a) Total power consumption of the four robots

b) Standard deviation of the robots' power consumption

Fig. 18 Energy consumption performance of the rotorcraft.

Table 5 Comparison of energy consumption performance

Quantity	Case 1	Case 2
Average cable tension variance (N^2)	**0.0076**	0.2092
Average individual robot power (W)	**189.14**	191.44
Average total power (W)	**756.7**	765.8
Average power std (W)	**6.011**	7.642

VI. Conclusions

A load-distribution-based trajectory planning and control strategy for a hierarchically controlled multilift system is studied in this paper. A method that simultaneously plans payload trajectory and cable forces while satisfying path and force constraints and minimizing the difference in cable forces is proposed. Direct collocation method is used to solve the formulated planning problem. Then, a neighboring feedback law is then designed to equalize the cable tension load distribution for the real flight. The system dynamics are linearized about the nominal path. An linear-quadratic regulator (LQR) controller is then designed for the system to track the planned trajectory

Both numerical simulation and hardware flight experiments are performed to validate the proposed approach. Three test cases for planning are considered in the simulation: with the given final time $t_f = 5.0$, 2.8, and 2.3 s. A 2.5 m/s wind gust is added to the environment to test the effectiveness of the tracking control by applying the designed neighboring feedback controller. Simulation results showed that, by reducing the arriving time, all the cable tensions increase but still with a evenly distributed load. The payload ended with a larger rotation maneuver and a more aggressive change of sector angle in order to achieve the goal in a shorter time by bigger acceleration. Even with the effect of disturbances (i.e., wind gusts), cable tensions are more evenly distributed with the proposed approach.

Flight results from hardware implementation performed in a Vicon motion capture studio are presented. Two cases were tested and compared: one with the proposed load-distribution-based planning and the neighboring feedback control approach, and the other with the polynomial curve planning method and the hierarchical approach with cable force computation. Results showed that the payload can be transported to the desired waypoint in both cases. The rotorcraft behaving as the actuators can effectively execute the payload command and track the commanded position. However, comparison showed that the system has reduced energy consumption in the case with planning based on load distribution. The rotorcraft achieved less variant cable tension, less average total power, and near-equal energy consumption as compared with the case without planning based on load distribution.

Appendix: Necessary Condition and Controller Parameters

A. Necessary Condition of the Planning Problem

The necessary conditions on $H_u = 0$ leads to the following system of equation:

$$H_u = L_u + f_u^T \boldsymbol{\lambda} = 0 \tag{A1}$$

where $\boldsymbol{\lambda}$ is the costate, and $L = (1/4)\sum_{i=1}^4 [T_i - (1/4)\sum_{j=1}^4 T_j]^2$, which is the cable tension variance at each time. The necessary conditions on $H_u = 0$ leads to the following system of equation:

$$H_u = L_u + f_u^T \boldsymbol{\lambda} \tag{A2}$$

where

$$L_{u_k} = \begin{cases} \dfrac{3}{8}T_i - \dfrac{1}{8}\displaystyle\sum_{j\neq i} T_j, & k = 2i-1, i, j = 1,2,3,4 \\ 0, & k = 2i \end{cases}$$

$$f_u = \begin{bmatrix} \mathbf{0}_{6\times 8} \\ --- \\ \boldsymbol{E}_{6\times 8} \end{bmatrix} \tag{A3}$$

where the $2i-1$th column of $\boldsymbol{E}$ is

$$\boldsymbol{e}_{2i-1} = \begin{bmatrix} \frac{R_{11}\sin\alpha\cos\beta_i + R_{12}\sin\alpha\sin\beta_i - R_{13}\cos\alpha}{m} \\ \frac{R_{21}\sin\alpha\cos\beta_i + R_{22}\sin\alpha\sin\beta_i - R_{23}\cos\alpha}{m} \\ \frac{R_{31}\sin\alpha\cos\beta_i + R_{32}\sin\alpha\sin\beta_i - R_{33}\cos\alpha}{m} \\ \frac{-g_{iy}\cos\alpha - g_{iz}\sin\alpha\sin\beta_i}{J_{xx}} \\ \frac{g_{iz}\sin\alpha\cos\beta_i + g_{ix}\cos\alpha}{J_{yy}} \\ \frac{g_{ix}\sin\alpha\sin\beta_i - g_{iy}\sin\alpha\cos\beta}{J_{zz}} \end{bmatrix} \tag{A4}$$

the $2i$th column of $\boldsymbol{E}$ is

$$\boldsymbol{e}_{2i} = \begin{bmatrix} \frac{-R_{11}T_i\sin\alpha\sin\beta_i + R_{12}T_i\sin\alpha\cos\beta_i}{m} \\ \frac{-R_{12}T_i\sin\alpha\sin\beta_i + R_{22}T_i\sin\alpha\cos\beta_i}{m} \\ \frac{-R_{31}T_i\sin\alpha\sin\beta_i + R_{32}T_i\sin\alpha\cos\beta_i}{m} \\ \frac{-g_{iz}T_i,\sin\alpha\cos\beta_i}{J_{xx}} \\ \frac{-g_{iz}T_i,\sin\alpha\sin\beta_i}{J_{yy}} \\ \frac{g_{ix}T_i\sin\alpha\cos\beta_i + g_{iy}T_i\sin\alpha\sin\beta_i}{J_{zz}} \end{bmatrix} \tag{A5}$$

where R_{ij} is the component of the rotation matrix from frame $\mathcal{F}_L$ to frame $\mathcal{F}_e$, and $\boldsymbol{g}_i$ is the cable attachment geometry vector of the ith cable. The necessary conditions on $\dot{\boldsymbol{\lambda}} = -H_x$ gives

$$\dot{\lambda}_1 = 0 \tag{A6}$$

$$\dot{\lambda}_2 = 0$$

$$\dot{\lambda}_3 = 0$$

$$\begin{aligned} -\dot{\lambda}_4 = {} & \lambda_4(\omega_y\cos\phi\tan\theta - \omega_z\sin\phi\tan\theta) \\ & + \lambda_5(-\omega_y\sin\phi - \omega_z\cos\phi) + \lambda_6\left(\omega_y\frac{\cos\phi}{\cos\theta} - \omega_z\frac{\sin\phi}{\cos\theta}\right) \\ & + \frac{\lambda_7}{m}\Big[(\sin\phi\sin\psi + \cos\phi\sin\theta\cos\psi)F_{Ty} \\ & + (\cos\phi\sin\psi - \sin\phi\sin\theta\cos\psi)F_{Tz}\Big] \\ & + \frac{\lambda_8}{m}\Big[-\sin\phi\cos\psi + \cos\phi\sin\theta\sin\psi)F_{Ty} \\ & - (\cos\phi\cos\psi + \sin\phi\sin\theta\sin\psi)F\tau_z\Big] \\ & + \frac{\lambda_9}{m}\Big[\cos\phi\cos\theta F_{Ty} - \sin\phi\cos\theta F_{Tz}\Big] \end{aligned} \tag{A7}$$

$$\begin{aligned} -\dot{\lambda}_5 = {} & \lambda_4\left(\omega_y\frac{\sin\phi}{\cos^2\theta} + \omega_z\frac{\cos\phi}{\cos^2\theta}\right) + \lambda_6\left(\omega_y\frac{\sin\phi}{\cos^2\theta}\sin\theta + \omega_z\frac{\cos\phi}{\cos^2\theta}\sin\theta\right) \\ & + \frac{\lambda_7}{m}\Big(-\sin\theta\cos\psi F_{Tx} + \sin\phi\cos\theta\cos\psi F_{Ty} + \cos\phi\cos\theta\cos\psi F_{Tz}\Big) \\ & + \frac{\lambda_8}{m}\Big[-\sin\theta\sin\psi F_{Tx} + \sin\phi\cos\theta\cos\psi F_{Ty} + \cos\phi\cos\theta\cos\psi F_{Tz}\Big] \\ & + \frac{\lambda_9}{m}\Big[-\cos\theta F_{Tx} - \sin\phi\sin\theta F_{Ty} - \cos\phi\sin\theta F_{Tz}\Big] \end{aligned} \tag{A8}$$

$$\begin{aligned} -\dot{\lambda}_6 = {} & \frac{\lambda_7}{m}\Big[-\cos\psi F_{Tx} - (\cos\phi\cos\psi + \sin\phi\sin\theta\sin\psi)F_{Ty} \\ & + (\sin\phi\cos\psi - \cos\phi\sin\theta\sin\psi)F_{Tz}\Big] \\ & + \frac{\lambda_8}{m}\Big[\cos\theta\cos\psi F_{Tx} + (-\cos\phi\sin\psi + \sin\phi\sin\theta\cos\psi)F_{Ty} \\ & + (\sin\phi\sin\psi + \cos\phi\sin\theta\cos\psi)F_{Tz}\Big] \end{aligned} \tag{A9}$$

where F_{Ti} is the component of the total cable force acting on the payload center of mass in the body frame.

$$\dot{\lambda}_7 = -\lambda_1 \tag{A10}$$

$$\dot{\lambda}_8 = -\lambda_2$$

$$\dot{\lambda}_9 = -\lambda_3$$

$$-\dot{\lambda}_{10} = \lambda_4 + \lambda_{11}\frac{J_{zz} - J_{xx}}{J_{yy}}\omega_z + \lambda_{12}\frac{J_{xx} - J_{yy}}{J_{zz}}\omega_y \tag{A11}$$

$$\begin{aligned} -\dot{\lambda}_{11} = {} & \lambda_4(\sin\phi + \tan\theta) + \lambda_5\cos\phi + \lambda_6\frac{\sin\phi}{\cos\theta} \\ & + \lambda_{10}\frac{J_{yy} - J_{zz}}{J_{xx}}\omega_z + \lambda_{12}\frac{J_{xx} - J_{yy}}{J_{zz}}\omega_x \end{aligned} \tag{A12}$$

$$\begin{aligned} -\dot{\lambda}_{12} = {} & \lambda_4\cos\phi\tan\theta - \lambda_5\sin\phi + \lambda_6\frac{\cos\phi}{\cos\theta} \\ & + \lambda_{10}\frac{J_{yy} - J_{zz}}{J_{xx}}\omega_y + \lambda_{11}\frac{J_{zz} - J_{xx}}{J_{yy}}\omega_x \end{aligned} \tag{A13}$$

B. Controller Parameters for Hardware Implementation

Based on [22,23], the maximum desired state deviation from the nominal state can be selected as

$$dx = dy = dz = 0.14\ \mathrm{m} \tag{B1}$$

$$d\phi = d\theta = d\psi = 5\ \deg \tag{B2}$$

$$dv_x = dv_y = dv_z = 0.15\ \mathrm{m/s} \tag{B3}$$

$$dp = dq = dr = 20\ \deg/\mathrm{s} \tag{B4}$$

Similarly, the maximum allowable input deviations from the nominal input are chosen as

$$dT_i = 0.07\ \mathrm{N}, \qquad i = 1, 2, \ldots, 4 \tag{B5}$$

$$d\beta_i = 0.5\ \deg \tag{B6}$$

The matrices Q and R can then be designed based on the Bryson's rule:

$$q_{ii} = \frac{1}{\max(x_i)^2}, \qquad i = 1, 2, \ldots, 12 \tag{B7}$$

$$r_{jj} = \frac{1}{\max(u_j)^2}, \qquad j = 1, 2, \ldots, 8 \tag{B8}$$

which are

$$Q = \mathrm{diag}[51.02, 51.02, 51.02, 131.31, 131.31, 131.31, 44.44, 44.44, 44.44, 8.21, 8.21, 8.21] \tag{B9}$$

$$R = \mathrm{diag}[204.08, 13131.23, 204.08, 13131.23, 204.08, 13131.23, 204.08, 13131.23] \tag{B10}$$

where "diag" is the function to generate a diagonal matrix using the given vector as each of the diagonal entry, and with all the rest of the entries of the matrix to be zero.

Acknowledgments

This research was partially funded by the U.S. government under Agreement No. W911 W6-17-2-0003. The U.S. government is authorized to reproduce and distribute reprints for government purposes notwithstanding any copyright notation thereon. The views and conclusions contained in this document are those of the authors and should not be interpreted as representing the official policies, either expressed or implied, of the Aviation Development Directorate or the U.S. government.

References

[1] Fink, J., Michael, N., Kim, S., and Kumar, V., "Planning and Control for Cooperative Manipulation and Transportation with Aerial Robots," *International Journal of Robotics Research*, Vol. 30, No. 3, 2011, pp. 324–334.
https://doi.org/10.1177/0278364910382803

[2] Klausen, K., Fossen, T. I., Johansen, T. A., and Aguiar, A. P., "Cooperative Path-Following for Multirotor UAVS with a Suspended Payload," *2015 IEEE Conference on Control Applications (CCA)*, Inst. of Electrical and Electronics Engineers, New York, 2015, pp. 1354–1360.
https://doi.org/10.1109/CCA.2015.7320800

[3] Zhang, X., Zhang, F., Huang, P., Gao, J., Yu, H., Pei, C., and Zhang, Y., "Self-Triggered Based Coordinate Control with Low Communication for Tethered Multi-UAV Collaborative Transportation," *IEEE Robotics and Automation Letters*, Vol. 6, No. 2, 2021, pp. 1559–1566.

[4] Sreenath, K., and Kumar, V., "Dynamics, Control and Planning for Cooperative Manipulation of Payloads Suspended by Cables from Multiple Quadrotor Robots," *Proceedings of Robotics: Science and Systems*, Berlin, Germany, June 2013.
https://doi.org/10.15607/RSS.2013.IX.011

[5] Masone, C., Bülthoff, H. H., and Stegagno, P., "Cooperative Transportation of a Payload Using Quadrotors: A Reconfigurable Cable-Driven Parallel Robot," *2016 IEEE/RSJ International Conference on Intelligent Robots and Systems (IROS)*, Inst. of Electrical and Electronics Engineers, New York, 2016, pp. 1623–1630.
https://doi.org/10.1109/IROS.2016.7759262

[6] Lee, T., "Geometric Control of Quadrotor UAVs Transporting a Cable-Suspended Rigid Body," *IEEE Transactions on Control Systems Technology*, Vol. 26, No. 1, 2018, pp. 255–264.
https://doi.org/10.1109/TCST.2017.2656060

[7] Li, G., Ge, R., and Loianno, G., "Cooperative Transportation of Cable Suspended Payloads with MAVs Using Monocular Vision and Inertial Sensing," *IEEE Robotics and Automation Letters*, Vol. 6, No. 3, 2021, pp. 5316–5323.

[8] Li, Z., Horn, J. F., and Langelaan, J. W., "Coordinated Transport of a Slung Load by a Team of Autonomous Rotorcraft," *AIAA Guidance, Navigation, and Control Conference*, AIAA Paper 2014-0968, 2014.
https://doi.org/10.2514/6.2014-0968

[9] Enciu, J., and Horn, J. F., "Flight Performance Optimization of a Multilift Rotorcraft Formation," *Journal of Aircraft*, Vol. 54, No. 4, 2017, pp. 1521–1538.

[10] Berrios, M., Takahashi, M., Whalley, M., Schulein, G., Cicolani, L., and Powelll, J., "Load Distribution Control and Swing Angle Feedback for an Autonomous Dual Lift System with Flight Test Results," *74th Annual Forum of the American Helicopter Society*, American Helicopter Society, Phoenix, AZ, 2018.

[11] Bisgaard, M., "Modeling, Estimation, and Control of Helicopter Slung Load System," Ph.D. Thesis, Dept. of Control Engineering, Aalborg Univ., 2008.

[12] Bernard, M., and Kondak, K., "Generic Slung Load Transportation System Using Small Size Helicopters," *IEEE International Conference on Robotics and Automation, ICRA'09*, Inst. of Electrical and Electronics Engineers, New York, 2009, pp. 3258–3264.
https://doi.org/10.1109/ROBOT.2009.5152382

[13] Song, Y., Horn, J. F., Li, Z., and Langealaan, J. W., "Modeling, Simulation, and Non-Linear Control of a Rotorcraft Multi-Lift System," *Annual Forum Proceedings, 69th American Helicopter Society International Annual Forum*, Vol. 4, AHS International, Alexandria, VA, 2013, pp. 2695–2714.

[14] Klausen, K., Meissen, C., Fossen, T. I., Arcak, M., and Johansen, T. A., "Cooperative Control for Multirotors Transporting an Unknown Suspended Load Under Environmental Disturbances," *IEEE Transactions on Control Systems Technology*, Vol. 28, No. 2, 2020, pp. 653–660.
https://doi.org/10.1109/TCST.2018.2876518

[15] Michael, N., Fink, J., and Kumar, V., "Cooperative Manipulation and Transportation with Aerial Robots," *Autonomous Robots*, Vol. 30, No. 1, 2011, pp. 73–86.
https://doi.org/10.1007/s10514-010-9205-0

[16] Sanalitro, D., Savino, H. J., Tognon, M., Cortés, J., and Franchi, A., "Full-Pose Manipulation Control of a Cable-Suspended Load with Multiple UAVs Under Uncertainties," *IEEE Robotics and Automation Letters*, Vol. 5, No. 2, 2020, pp. 2185–2191.

[17] Bisgaard, M., la Cour-Harbo, A., Johnson, E. N., and Bendtsen, J. D., "Vision Aided State Estimator for Helicopter Slung Load System," *IFAC Proceedings Volumes*, Vol. 40, No. 7, 2007, pp. 425–430.
https://doi.org/10.3182/20070625-5-FR-2916.00073

[18] Bisgaard, M., la Cour-Harbo, A., and Bendtsen, J., "Full State Estimation for Helicopter Slung Load System," *AIAA Guidance, Navigation and Control Conference and Exhibit*, AIAA Paper 2007-6762, 2007.
https://doi.org/10.2514/6.2007-6762

[19] Mellinger, D., Lindsey, Q., Shomin, M., and Kumar, V., "Design, Modeling, Estimation and Control for Aerial Grasping and Manipulation," *2011 IEEE/RSJ International Conference on Intelligent Robots and Systems (IROS)*, Inst. of Electrical and Electronics Engineers, New York, 2011, pp. 2668–2673.
https://doi.org/10.1109/IROS.2011.6094871

[20] Geng, J., and Langelaan, J. W., "Estimation of Inertial Properties for a Multilift Slung Load," *Journal of Guidance, Control, and Dynamics*, Vol. 44, No. 2, 2021, pp. 220–237.
https://doi.org/10.2514/1.G005365

[21] Takahashi, M. D., Whalley, M. S., Schulein, G. J., and Berrios, M. G., "A System for Autonomous Rotorcraft Dual-Lift Flight Research,"

74th Annual Forum of the American Helicopter Society, American Helicopter Society, Phoenix, AZ, 2018.

[22] Geng, J., and Langelaan, J. W., "Implementation and Demonstration of Coordinated Transport of a Slung Load by a Team of Rotorcraft," *AIAA Guidance, Navigation, and Control Conference, AIAA Scitech 2019 Forum*, AIAA Paper 2019-0913, 2019.
https://doi.org/10.2514/6.2019-0913

[23] Geng, J., and Langelaan, J. W., "Cooperative Transport of a Slung Load Using Load-Leading Control," *Journal of Guidance, Control, and Dynamics*, Vol. 43, No. 7, 2020, pp. 1313–1331.
https://doi.org/10.2514/1.G004680

[24] Enciu, J., Horn, J. F., and Langelaan, J. W., "Formation Control of a Rotorcraft Multilift System," *Journal of the American Helicopter Society*, Vol. 62, No. 4, 2017, pp. 1–14.
https://doi.org/10.4050/JAHS.62.042011

[25] Li, Z., "Coordinated Transport of a Slung Load by a Team of Autonomous Rotorcraft," MS Thesis, Dept. of Aerospace Engineering, Pennsylvania State Univ., Dec. 2014.

[26] Bryson, A. E., and Ho, Y., *Applied Optimal Control: Optimization, Estimation and Control*, Taylor & Francis, 1975, pp. 148–149.

[27] Betts, J. T., "Survey of Numerical Methods for Trajectory Optimization," *Journal of Guidance, Control, and Dynamics*, Vol. 21, No. 2, 1998, pp. 193–207.
https://doi.org/10.2514/2.4231

[28] Adurthi, N., Singla, P., and Majji, M., "Sparse Approximation–Based Collocation Scheme for Nonlinear Optimal Feedback Control Design," *Journal of Guidance, Control, and Dynamics*, Vol. 40, No. 2, 2016, pp. 248–264.
https://doi.org/10.2514/1.G001755

[29] Kelly, M., "An Introduction to Trajectory Optimization: How to do Your Own Direct Collocation," *SIAM Review*, Vol. 59, No. 4, 2017, pp. 849–904.
https://doi.org/10.1137/16M1062569

E. Atkins
Associate Editor